Journal of Power Sources 273 (2015) 663–669

Contents lists available at ScienceDirect

Journal of Power Sources

journal homepage: www.elsevier.com/locate/jpowsour

Effect of outer layer thickness on full concentration gradient layered cathode material for lithium-ion batteries

Eung-Ju Lee [a], Hyung-Joo Noh [a], Chong S. Yoon [b], Yang-Kook Sun [a, *]

[a] Department of Energy Engineering, Hanyang University, Seoul 133-791, South Korea
[b] Department of Materials Science and Engineering, Hanyang University, Seoul 133-791, South Korea

HIGHLIGHTS

- $Li[Ni_{0.6-x}Co_{0.15+x}Mn_{0.25}]O_2$ with full concentration gradient was synthesized.
- Cathodes were coated with different outer layer thickness having a constant composition.
- Thicker outer layer improved cycle performance and thermal stability.
- Thicker outer layer undermined the rate capability.
- Outer layer coating can be selectively used for specific requirements.

GRAPHICAL ABSTRACT

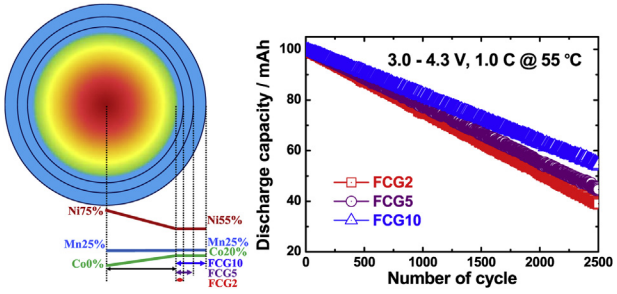

ARTICLE INFO

Article history:
Received 4 September 2014
Received in revised form
24 September 2014
Accepted 25 September 2014
Available online 2 October 2014

Keywords:
Layered oxide
Cathode
Full concentration gradient
Rate capability
Lithium-ion batteries

ABSTRACT

Full concentration gradient (FCG) layered cathode materials $Li[Ni_{0.6-x}Co_{0.15+x}Mn_{0.25}]O_2$ ($x = 0$, 0.01, and 0.04) with different outer layer thicknesses are synthesized via a specially developed coprecipitation method. In the FCG cathode, the nickel concentration decreases linearly and the cobalt concentration increases from the center to particle surface throughout the particle at a fixed composition of Mn. The thickness of the FCG primary particle increases in the radial direction with an increasing outer layer thickness of the secondary particles and significantly affects the electrochemical performance. An increase in the stable outer layer thickness improves the cycle performance and thermal stability of the FCG materials at the expense of reversible capacity, whereas the rate capability and low temperature performance are significantly deteriorated by increasing outer layer thickness. All of the FCG materials exhibit superior electrochemical and thermal properties compared to the conventional cathode $Li[Ni_{0.58}Co_{0.17}Mn_{0.25}]O_2$ due to the unique microstructure of the FCG cathode.

1. Introduction

Over the past decade, much attention has been paid to layered Ni-rich $Li[Ni_{1-x}M_x]O_2$ (M = transition metal, $x \leq 0.2$) as a promising cathode material for lithium-ion batteries because of their potentially high reversible capacity, good rate capability, and relatively low cost [1–4]. However, $Li[Ni_{1-x}M_x]O_2$ materials suffer from poor cycling performance and thermal safety because of the high concentration of relatively reactive Ni^{4+} when charged to greater than 4.2 V and the oxygen release from the highly delithiated electrode, especially at elevated temperature [1,2]. To overcome these problems of layered Ni-rich materials, Co and/or Mn and Al have been substituted for Ni to form $Li[Ni_{0.8}Co_{0.15}Al_{0.05}]O_2$ and $Li[Ni_{0.8}Co_{0.1}Mn_{0.1}]O_2$ [3,5–7]. While these materials have shown improved electrochemical properties, the cycling performance and thermal stability should be further improved for practical battery applications.

* Corresponding author.
E-mail addresses: yksun@hanyang.ac.kr, yksun7804@gmail.com (Y.-K. Sun).

http://dx.doi.org/10.1016/j.jpowsour.2014.09.161
0378-7753/

It is well-known that an increase in Ni concentration in Li $[Ni_{1-x}M_x]O_2$ increases the reversible capacity, whereas an increase in Mn content yields better cycle life and thermal stability at the expense of reversible capacity [8,9]. We recently reported synthesis of a Ni-enriched cathode material with a layered structure and a full concentration gradient (FCG). The FCG cathode was spherical in shape, with the Ni concentration decreasing gradually from the particle center toward the surface, while the Mn concentration increased linearly from the core. The FCG produced the Ni-enriched particle core and the Mn-enrich outer layer without an abrupt change in composition and imparted both high capacity and outstanding safety performance to the Ni-enriched cathode [10–13]. In addition, FCG material has a unique microstructure composed of long rod-shaped primary particles radiating from the particle center. The rod-shaped primary particles are responsible for the excellent cycle performance, thermal stability, and lower temperature performance by reducing the exposed contact area with the liquid electrolyte due to the lower specific surface area and the enhanced Li^+ diffusion through the material [11,12].

Here, we report the effect of an outer layer with a constant composition encapsulating the FCG cathode, which is schematically described in Fig. 1. The particle center ($[Ni_{0.75}Mn_{0.25}](OH)_2$) and outer surface compositions ($[Ni_{0.55}Co_{0.20}Mn_{0.25}](OH)_2$) in the hydroxide precursor are fixed, as shown in Fig. 1. The particle had a linearly decreasing Ni concentration from 75% to 55% toward the particle outer surface, while the Co concentration increased from 0% to 20% at a fixed Mn concentration. The FCG hydroxide particle was encapsulated with an outer layer having a constant composition of $[Ni_{0.55}Co_{0.20}Mn_{0.25}](OH)_2$ with three different thicknesses. The long-term cycling performance and thermal properties of the FCG material with an outer layer were evaluated as a function of the outer layer thickness (0.2, 0.5, and 1.0 μm). Hereafter, the FCG materials with outer layer thickness 0.2, 0.5, and 1.0 μm are denoted as FCG2, FCG5, and FCG10, respectively. For comparison, the electrochemical performances and thermal properties of the conventional cathode (CC, $Li[Ni_{0.58}Co_{0.17}Mn_{0.25}]O_2$) without a concentration gradient were also evaluated.

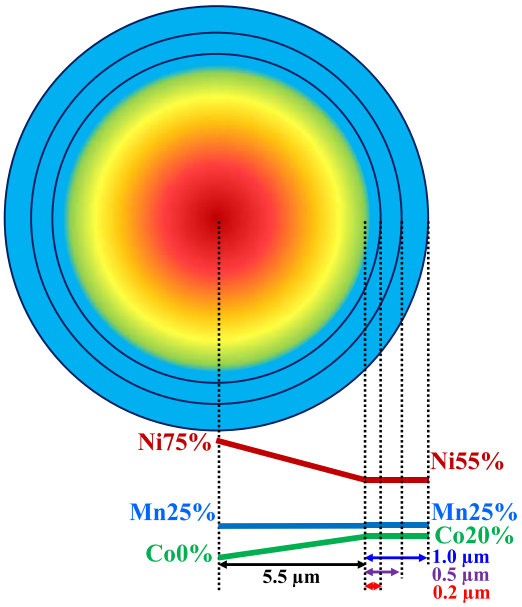

Fig. 1. Schematic diagram of the FCG hydroxide precursor with different outer layer thicknesses. The variation in concentration within the FCG hydroxide precursor with different outer layer thicknesses.

2. Experimental

2.1. Synthesis of CC $Li[Ni_{0.58}Co_{0.17}Mn_{0.25}]O_2$

The $[Ni_{0.58}Co_{0.17}Mn_{0.25}](OH)_2$ precursor was synthesized via co-precipitation of $NiSO_4 \cdot 6H_2O$, $CoSO_4 \cdot 7H_2O$, and $MnSO_4 \cdot 5H_2O$ (58:17:25 in molar ratio) as starting materials. Details of the preparation procedures are given in a previous report [14]. The obtained $[Ni_{0.58}Co_{0.17}Mn_{0.25}](OH)_2$ hydroxide precursor was mixed with $LiOH \cdot H_2O$ and calcined at 870 °C for 10 h in air.

2.2. Synthesis of FCG2, FCG5, and FCG10

To prepare the FCG2, FCG5, and FCG10, at the starting of a continuously stirred tank reactor (CSTR, 4L) operation, $NiSO_4 \cdot 6H_2O$ and $MnSO_4 \cdot 5H_2O$ (Ni:Mn = 0.75:0.25 in molar ratio) solution (1.2 mol L^{-1}) from a tank 1 was slowly pumped into the CSTR. Concurrently, a Ni-deficient aqueous solution (Ni:Co:Mn = 0.50:0.25:0.25 in molar ratio) from a tank 2 made of $NiSO_4 \cdot 6H_2O$, $CoSO_4 \cdot 7H_2O$, and $MnSO_4 \cdot 5H_2O$ was slowly pumped into the Ni-rich (Ni:Mn = 0.75:0.25) stock solution in the tank 1, after which the homogeneously mixed solution was fed into the CSTR [10–12,15]. Simultaneously, a 4.0 mol L^{-1} NaOH solution (aq) (molar ratio of ammonium hydroxide to transition metal = 1.0) and the desired amount of a NH_4OH (2.0 mol L^{-1} solution (aq), molar ratio of sodium hydroxide to transition metal = 2.0) were pumped separately into the reactor. After the composition of tank 1 reached the desired surface composition, the feeding of tank 2 was stopped, and a controlled surface composition from tank 1 was continuously pumped to CSTR for 2 h, 4 h, or 8 h. The co-precipitated hydroxide precursor powders were filtered, washed with deionized water, and dried at 110 °C. The obtained FCG2, FCG5, and FCG10 hydroxide precursors were mixed with $LiOH \cdot H_2O$, and the mixtures were calcined at 825, 845, or 875 °C for 10 h in air, respectively.

2.3. Material characterizations

The chemical compositions of the prepared powders were determined by atomic absorption spectroscopy (AAS, Vario 6, Analyticjena). The morphology of each powder was observed with scanning electron microscopy (SEM, JSM 6400, JEOL). To obtain the localized composition of the materials at particle level, cross-sections of the particles were prepared by embedding them in an epoxy and grinding them flat. Line scans of the polished surfaces for the prepared FCG hydroxide precursors and lithiated oxides were analyzed by an electron probe micro-analyzer (EPMA) (JXA-8100, JEOL).

2.4. Electrochemical test

For fabrication of the cathodes, the synthesized powders were mixed with carbon black and polyvinylidene fluoride (85:7.5:7.5) in *N*-methylpyrrolidinone. The obtained slurry was coated onto Al foil and roll-pressed. Fundamental cell tests were performed with a 2032 coin-type cell using Li metal as the anode cycled from 2.7 to 4.4 V. Long-term cycle-life tests were performed in a laminated-type full cell (36 mAh) wrapped with an Al pouch. Mesocarbon microbead graphite (MCMB, Osaka Gas) was used as the anode. The electrode size of the full cell was 3 cm × 5 cm. The electrolyte solution was 1.2 M $LiPF_6$ in ethylene carbonate–ethyl-methyl carbonate (3:7 in volume). The cells were charged and discharged at 25 °C and 55 °C, respectively, between 3.0 and 4.3 V by applying a constant 1C current (36 mA corresponds to 200 mA g^{-1}).

2.5. Thermal properties

For the differential scanning calorimetry (DSC) experiments, the FCGs and CCSC electrodes were charged to 4.3 V versus Li and disassembled in an Ar-filled dry box. A stainless-steel-sealed pan with a gold-plated copper seal was used to collect 3–5 mg samples. Measurements were carried out in a DSC 200 PC (NETZSCH, Germany) using a temperature scan rate of 5 °C min^{-1}.

3. Results and discussion

The total chemical compositions of the as-prepared FCG2, FCG5, and FCG10 were found to be $Li[Ni_{0.60}Co_{0.15}Mn_{0.25}]O_2$, $Li[Ni_{0.59}Co_{0.16}Mn_{0.25}]O_2$, and $Li[Ni_{0.56}Co_{0.19}Mn_{0.25}]O_2$, respectively, as determined by AAS. The compositional variations of the Ni and Co on the cross-section of a single particle were measured by an EPMA with a probe diameter of 100 nm, and the results are shown in Fig. 2. As per the design, the Mn concentration across the single precursor particle was constant at 25 at % throughout the entire particle. The Ni concentration decreased gradually from 75 at % to 55 at % toward the particle surface, while the Co concentration increased from 0 at % to 20 at % for all the three hydroxide precursors. In addition to the concentration gradient, the outer shell thickness with constant composition for the FCG2, FCG5, and FCG10 hydroxide precursors was clearly observed near the particle surface. The estimated outer layer thickness was 0.2, 0.5, to 1.0 μm for the FCG2, FCG5, FCG10 hydroxide precursors, respectively, satisfying the planned material design. Interdiffusion of transition metal ions within the particle during the high-temperature calcination had little effect on the outer surface composition of the lithiated oxide, as shown in Fig. 2d,e and f. The outer surface compositions of the FCG2, FCG5, and FCG10 lithiated oxides were $Li[Ni_{0.58}Co_{0.17}Mn_{0.25}]O_2$, $Li[Ni_{0.57}Co_{0.18}Mn_{0.25}]O_2$, and $Li[Ni_{0.55}Co_{0.20}Mn_{0.25}]O_2$, respectively. However, the outer surface thickness with a constant composition in the lithiated oxide was increased with increasing outer layer shell thickness in hydroxide precursor. Furthermore, the Ni concentration in the particle center decreased slightly to 70 at %, whereas the Co concentration increased to 5 at %, resulting in a particle center composition of $Li[Ni_{0.70}Co_{0.05}Mn_{0.25}]O_2$.

SEM images of the synthesized FCGs powders are shown in Fig. 3. All of the observed particles had a spherical morphology with an average particle diameter of 12 μm. Each particle was composed of micrometer-sized (1–3 μm) elongated primary particles [11,12]. The thickness of the primary particle in the radial direction increased with an increasing outer layer thickness of the secondary particles, which can improve cycle life and thermal properties by reducing chemical activity with liquid electrolyte. Fig. 4 shows a typical TEM image of the FCG cathode (FCG5) whose TEM sample was prepared by focused ion beam. Rod-shaped primary particles extending the center to the particle surface were clearly observed. It is also noted that an outer layer with a constant composition did not affect the particle morphology as no kinks or discontinuity were observed near the boundary between the outer layer and the end of the FCG. In addition to the long rod-shaped morphology, similar to the previously synthesized FCG cathode, each primary particle exhibited a strong crystallographic texture, confirmed by electron diffraction (data not shown). The layered planes within each primary particle were aligned parallel to the longitudinal direction of the primary particle, i.e., the layer planes were also radially oriented such that Li^+ ion diffusion into and out of the cathode particle was accelerated [11]. Similar morphology was also observed from FCG2 and FCG10.

The fundamental electrochemical properties of the materials were tested in 2032 coin-type half-cells employing Li metal as the anode, and the results are shown in Fig. 5. The outer layer composition of CC $Li[Ni_{0.58}Co_{0.17}Mn_{0.25}]O_2$ was also tested for comparison. Fig. 5a shows the initial charge–discharge curves for the FCG2, FCG5, FCG10, and CC between 3.0 V and 4.4 V with a constant current density of 20 mA g^{-1} (0.1C rate) at 25 °C. The initial discharge capacity of the cathodes decreased with increasing outer shell thickness due to the reduced concentration of the most active redox Ni ions; 201 mAh g^{-1} for FCG2, 196 mAh g^{-1} for FCG5, and 192 mAh g^{-1} for FCG10. Note that the CC $Li[Ni_{0.58}Co_{0.17}Mn_{0.25}]O_2$ electrode delivered the lowest discharge capacity of

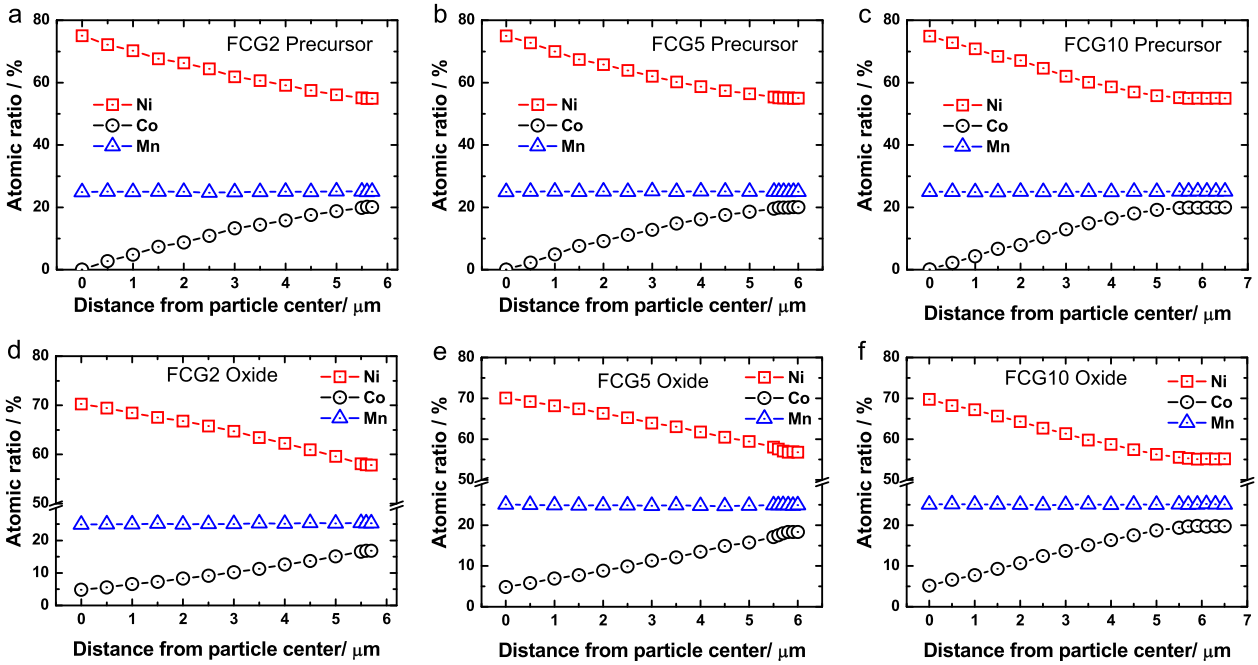

Fig. 2. EPMA line scan of the integrated atomic ratio of transition metals as a function of the distance from the particle center to the surface for FCG $[Ni_{0.6-x}Co_{0.15+x}Mn_{0.25}](OH)_2$, (a) $x = 0.0$, (b) $x = 0.01$, and (c) $x = 0.04$, and for FCG $Li[Ni_{0.6-x}Co_{0.15+x}Mn_{0.25}]O_2$, (d) $x = 0.0$, (e) $x = 0.01$, and (f) $x = 0.04$.

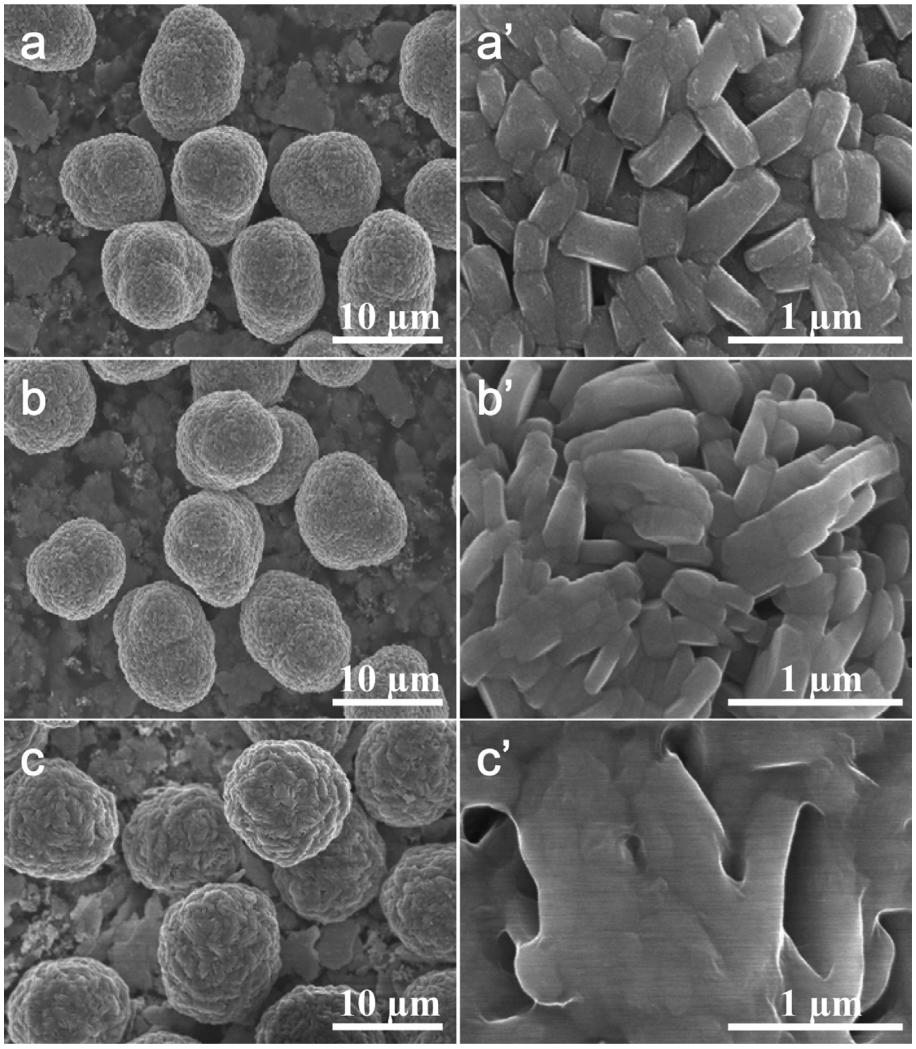

Fig. 3. SEM images of FCG $Li[Ni_{0.6-x}Co_{0.15+x}Mn_{0.25}]O_2$; (a) $x = 0.0$, (b) $x = 0.01$, and (c) $x = 0.04$, where the images on the right show the magnified images of the corresponding samples.

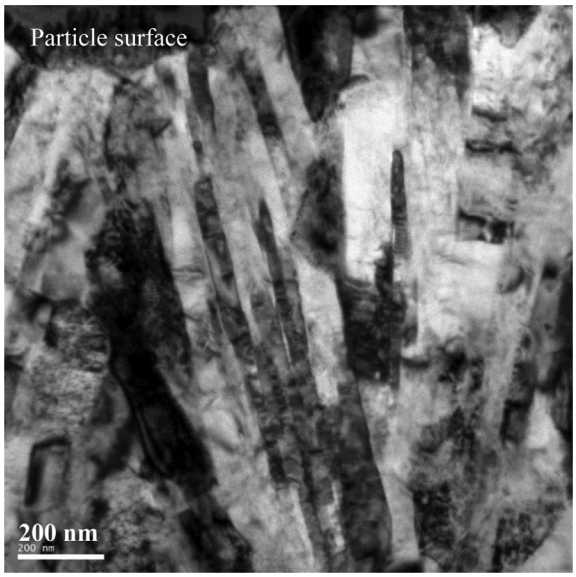

Fig. 4. TEM image of the FCG5 cathode in the as-prepared state prior to electrochemical cycling.

186 mAh g^{-1} though the Ni content (58 at %) in the CC was larger than that (56 at %) of FCG10. As reported in our previous papers [11], the higher Ni^{2+} concentration in FCG was responsible for the larger discharge capacity.

However, as shown in Fig. 5b, the capacity retention of the FCG materials increased with increasing outer layer thickness; 92.1% for FCG2, 92.4% for FCG5, and 94.1% for FCG10 after 100 cycles. The increased capacity retention is due to the decreased Ni concentration on the particle outer surface. A striking feature is that, considering the Ni content (0.58) of the CC material, the lowest capacity retention (87.7%) of CC was unexpected compared with those of FCG2 (Ni content of 0.60) and FCG5 (0.59). All the tested FCG materials here showed better electrochemical performances than CC in terms of capacity and cycle life due to the unique rod-shaped morphology of the primary particles with the concentration gradient [11,12].

We fabricated an Al pouch-type full cell (capacity of 36 mAh) with FCGs as the cathode and mesocarbon microbeads (MCMB, graphite) as the anode in order to investigate the long-term cycling performance. Fig. 6 shows the discharge capacity versus the number of cycles for the C/FCGs cells cycled at 25 °C and 55 °C between 3.0 and 4.3 V by applying a constant current of 1C rate (36 mA). As anticipated, the cycle life of the FCG cathodes increased with

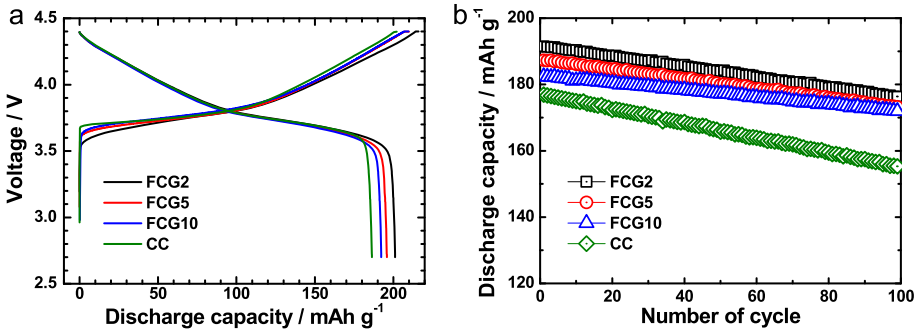

Fig. 5. (a) Initial charge–discharge curves of the FCG $Li[Ni_{0.6-x}Co_{0.15+x}Mn_{0.25}]O_2$ obtained from 2032 coin-type half-cells at 25 °C using Li metal as the anode (current density at a 0.1C rate corresponding to 20.0 mA g^{-1}), and (b) corresponding cycling performance of the half-cells between 2.7 and 4.3 V by applying a constant current at a 0.5C rate (100 mA g^{-1}).

increasing outer layer thickness, showing capacity retention of 76.5%, 77.7%, and 82.5% for FCG2, FCG5, and FCG10, respectively. This trend was unequivocally evident at more aggressive test condition of cycling at 55 °C. The FCG10 showed the best capacity retention of 54.4% after 2500 cycles, even at 55 °C, while capacity retention of FCG2 and FCG5 reached only 39% and 44.7%, respectively. We believe that the excellent cycling performance of FCG10 is mainly due to the reduced concentration of unstable Ni on the particle outer layer surface, in agreement with our previous report of the increased Mn and reduced Ni concentrations in the particle surface with rod-shaped morphology [10–13,16].

To confirm the effect of the outer layer on the structure of the FCG electrodes after the extended cycling, the cycled electrodes (after 2500 cycles at 55 °C) were recovered from the full cell and analyzed using TEM. Fig. 7a shows a TEM image of the cycled FCG10 particle. In spite of the extended cycling at an elevated temperature, no noticeable damage was observed, unlike the CC electrode, which was pulverized after cycling [17]. The ends of the primary particles after cycling can be seen in Fig. 7b. As evident in the TEM image in Fig. 7b, the primary particles from the cycled FCG10 electrode retained the initial rod-shaped morphology and crystallographic texture. The electron diffraction in Fig. 7b was indexed to the 120 zone of the hexagonal structure, and the c-axis of the lattice was aligned normal to the longitudinal axis of the primary particle. When the cycled FCG2 electrode was examined by TEM, although the spherical morphology was maintained after 2500 cycles, the surface of the FCG2 electrode was permanently altered by the extended cycling at 55 °C, as can be seen in Fig. 7c. Instead of being terminated by the rod-shaped primary particle, the surface of the cycled FCG2 electrode was covered with small equi-axed primary particles (~200 nm in size), which were not observed in the pristine state. The electron diffraction images from such equi-axed primary particles, shown in Fig. 7d, illustrated a cubic structure as the diffraction was indexed to the 100 zone of a cubic structure. It appears that the surface of the FCG2 electrode was partially transformed from the layered structure to a cubic structure, as the four-fold symmetry observed in the electron diffraction image in Fig. 7d was non-existent in the layered hexagonal structure. The relatively poor capacity retention of the FCG2 cathode at 55 °C was likely ascribed to the structural damage incurred due to the relatively high concentration of Ni near the surface compared to that of the FCG10 electrode. The TEM analysis of the cycled electrodes suggests that a thick Mn-enriched outer layer encapsulating an FCG can extend the cycle life of the FCG cathode at an elevated temperature by reducing the relative concentration of Ni near the surface.

To further investigate the effect of particle outer layer thickness of the FCG materials, their rate and low temperature performances were characterized. Fig. 8a shows the rate capability of the FCGs and CC materials. Each cell was charged and discharged galvanostatically at different C rates ranging from 0.2 to 5C (40–1000 mA g^{-1}). As expected, the rate capability of the FCGs deteriorated faster with increasing outer layer thickness due to increased Mn concentration in the outer layer, in agreement with previous results [8,9]. The capacity difference among the FCGs and CC cathodes increased with increasing C rate. At a rate of 5C, the FCG2 delivered the highest discharge capacity of 143 mAh g^{-1}, while the FCG10 and CC achieved only 107 and 104 mAh g^{-1}, respectively. Particularly, FCG10 showed almost identical rate capability characteristics to the CC cathode due to the thick outer layer thickness of 1 μm. The low-temperature performance further confirmed the impact of the outer layer thickness, as shown in Fig. 8b. Similar to the rate capability characteristics, the low-temperature performance of FCGs worsened when the outer layer thickness increased. At −20 °C, the FCG2 delivered a high capacity

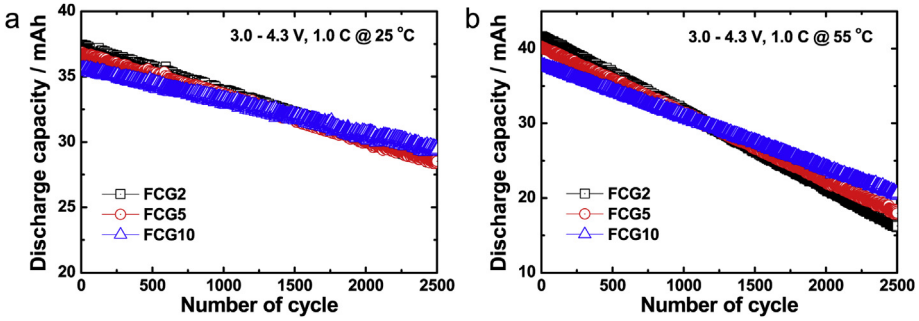

Fig. 6. Cycling performance of a laminated-type Al-pouch cell (36 mAh) using mesocarbon microbead (MCMB) graphite as the anode and FCGs as the cathode at a rate of 1C and (a) 25 °C and (b) 55 °C, corresponding to 200 mA g^{-1} (upper cutoff voltage of 4.3 V).

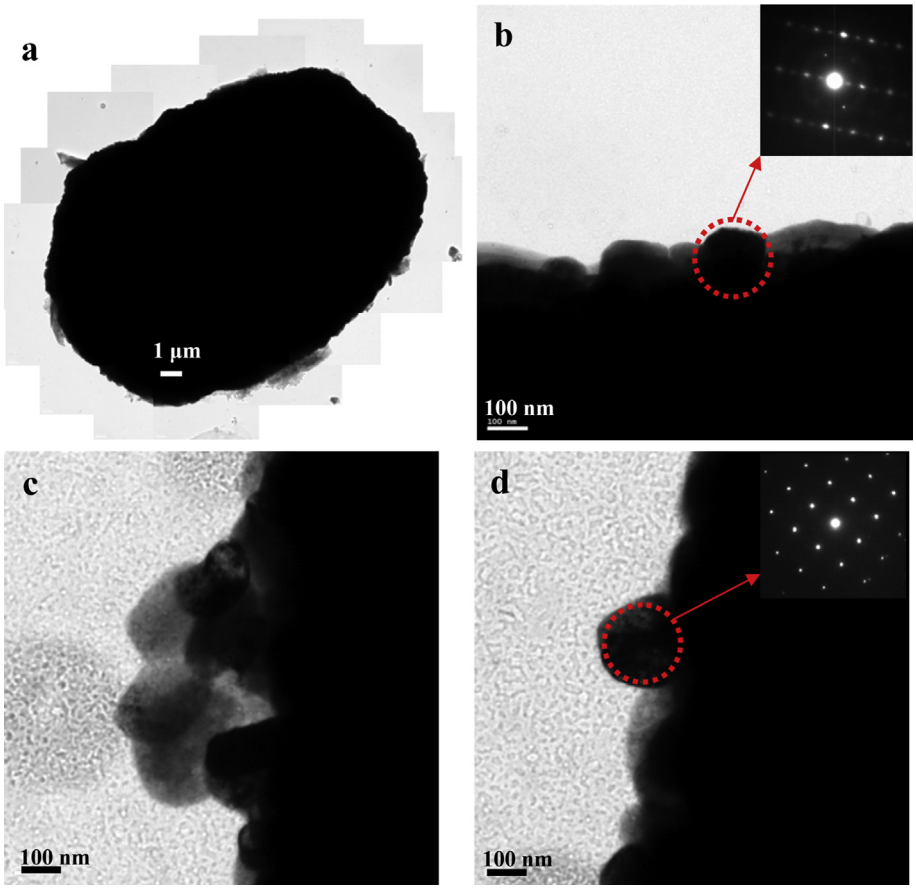

Fig. 7. TEM images of the cycled electrodes (a), (b) FCG10, and (c), (d) FCG2. The electrodes were cycled for 2500 cycles in laminated-type Al-pouch cells (36 mAh) using mesocarbon microbead (MCMB) graphite as the anode at 55 °C.

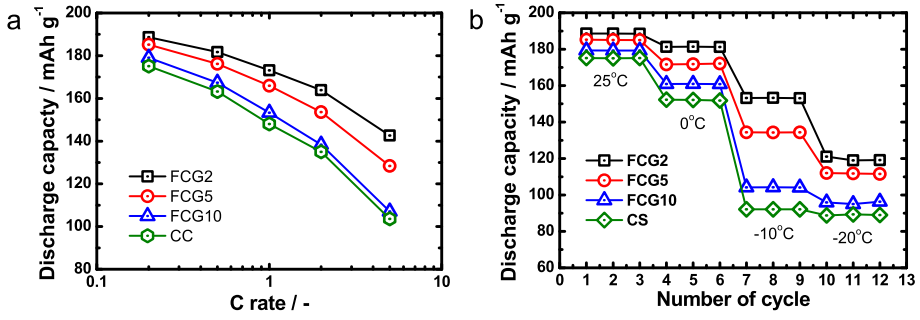

Fig. 8. Electrochemical performances of CC and FCG cathodes from a 2032 coin-type half-cells between 2.7 V and 4.3 V at 0.2C rate; (a) rate capabilities and (b) low-temperature performance.

of 116 mAh g^{-1}, which is higher than 95 and 90 mAh g^{-1} delivered by the FCG10 and CC cathodes, respectively. Thus, a thick outer layer can protect the FCG cathode from structural damage and enhance the cycle life but reduces the rate capability and low-temperature performance due to the longer diffusion path for Li^+ ions.

As a cross-validation, the electronic conductivity and Li^+ diffusivity of the FCGs and CC materials were evaluated and correlated with the electrochemical performances of the proposed materials. The electronic conductivity of the FCGs and CC materials was measured using a four-probe method, and the Li^+ diffusivity was determined using the galvanostatic intermittent titration method [18]. For the preparation of samples to measure electrical conductivity, the mixture of cathode powder and KBr binder was pressed to 340 atm and calcined at 600 °C for 15 h. As shown in Table 1, the electronic conductivity of the materials increased with decreasing outer layer thickness due to a higher amount of Ni in the outer layer [8]. The electronic conductivity for the FCG2 (6.3×10^{-5} S cm^{-1}) was one order of magnitude higher than that of CC materials

Table 1
Electronic conductivities of the CC and FCG $Li[Ni_{0.6-x}Co_{0.15+x}Mn_{0.25}]O_2$ ($x = 0.0$, 0.01, and 0.04).

	Electronic conductivity/S cm^{-1}
FCG2	6.30×10^{-5}
FCG5	5.84×10^{-5}
FCG10	1.34×10^{-5}
CC	3.68×10^{-6}

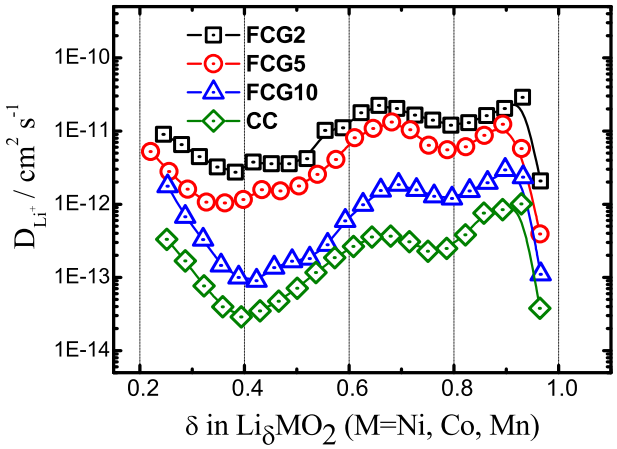

Fig. 9. Variation of the chemical diffusion coefficient, D_{Li^+}, of CC and FCG $Li[Ni_{0.6-x}Co_{0.15+x}Mn_{0.25}]O_2$ (x = 0.0, 0.01, and 0.04) as a function of charge state.

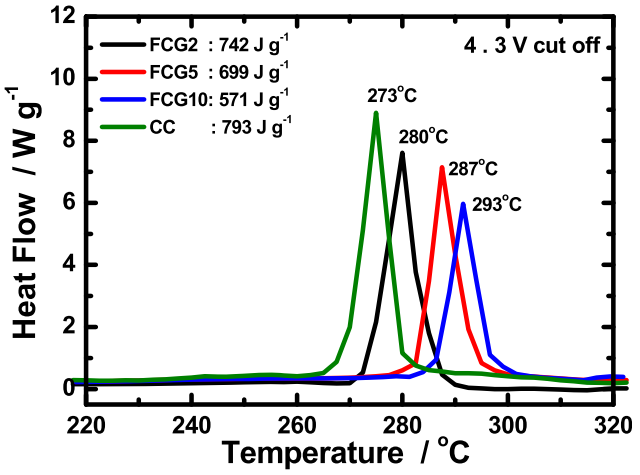

Fig. 10. DSC traces of the electrochemically delithiated CC and FCG $Li[Ni_{0.6-x}Co_{0.15+x}Mn_{0.25}]O_2$ (x = 0.0, 0.01, and 0.04) charged to 4.3 V.

(3.68×10^{-6} S cm^{-1}). Similarly, the Li^+ diffusivities of the materials increased with a decrease in outer layer thickness. As can be seen in Fig. 9, the Li^+ diffusivities of the FCG2 and FCG5 were almost 10 times higher than those for FCG10 and CC materials. Based on these results, the high rate capability and low-temperature performance were strongly dependent on both the electronic conductivity and Li^+ diffusivity.

To assess the thermal safety of the FCGs and CC cathode materials, the exothermic reaction temperature and the amount of heat released from the electrochemically delithiated cathodes were analyzed with DSC in the presence of electrolyte, and the results are shown in Fig. 10. The exothermic reaction peak of the FCGs shifted to a higher temperature from 280 °C for FCG2 to 293.4 °C for FCG10 and demonstrated reduction in heat generation (from 724 J g^{-1} to 571 J g^{-1}), again, due to the increased stable outer layer thickness. Meanwhile, the thermal stability of the CC $Li_{1-\delta}[Ni_{0.58}Co_{0.17}Mn_{0.25}]O_2$ was significantly reduced; it had an exothermic peak at 273 °C, generating 793 J g^{-1} of exothermic heat. Considering the Ni concentration of 0.58 in the CC, the thermal stability of the CC should be lie between FCG5 (0.59) and FCG10 (0.56). As observed, the improved thermal property of the FCG10 was caused by an increase in the thermally stable outer layer of $Li_{1-\delta}[Ni_{0.55}Co_{0.20}Mn_{0.25}]O_2$ by greatly stabilizing the near-surface region of the materials and thus limiting the surface chemical reactivity with the electrolyte.

4. Conclusions

We synthesized FCG $Li[Ni_{0.6-x}Co_{0.15+x}Mn_{0.25}]O_2$ (x = 0, 0.01, and 0.04) cathodes with different outer layer thicknesses of constant concentration via a coprecipitation method. The outer layer thickness strongly influenced both the electrochemical properties and thermal stability of the FCG materials. An increase in the stable outer layer thickness substantially improved the long-term cycling performance, as the capacity retention for the FCG10 reached 54.4%, but that of FCG2 showed only a 39% retention under aggressive test condition (between 3.0 V and 4.3 V after 2500 cycles at 55 °C). However, the rate capability and low temperature performance deteriorated at a faster rate with increase in the outer layer thickness. The improved cycle life and thermal property coinciding with increased outer layer thickness were attributed to the stabilization of the near-surface region of the FCG cathodes and thus limited the surface chemical reactivity with the electrolyte. Hence, it is proposed that the outer layer thickness of FCG materials should be selectively designed and synthesized based on the required application. In addition, all of the tested FCG cathodes showed superior electrochemical performances compared to the CC cathode in terms of electrochemical and thermal performances due to the unique rod-shaped morphology of the primary particles.

Acknowledgments

This work was mainly supported by the Global Frontier R&D Program (2013–073298) of the Center for Hybrid Interface Materials (HIM) funded by the Ministry of Science, ICT & Future Planning and was also supported by the Human Resources Development program (No. 20124010203290) through a Korea Institute of Energy Technology Evaluation and Planning (KETEP) grant funded by the Korean government Ministry of Trade, Industry and Energy.

References

[1] J.R. Dahn, E.W. Fuller, M. Obrovac, U. von Sacken, Solid State Ionics 69 (1994) 265–270.
[2] J. Shim, R. Kostecki, T. Richardson, X. Song, K.A. Striebel, J. Power Sources 112 (2002) 222–230.
[3] M.-H. Kim, H.-S. Shin, D. Shin, Y.-K. Sun, J. Power Sources 159 (2006) 1328–1333.
[4] B. Scrosati, J. Garche, J. Power Sources 195 (2010) 2419–2430.
[5] R.B. Wright, J.P. Christophersen, C.G. Motloch, J.R. Belt, C.D. Ho, V.S. Battaglia, J.A. Barnes, T.Q. Duong, R.A. Sutula, J. Power Sources 112 (2003) 865–869.
[6] R. Kostecki, F. McLarnon, Electrochem. Solid State Lett. 7 (2004) A380–A383.
[7] K.-S. Lee, S.-T. Myung, K. Amine, H. Yashiro, Y.-K. Sun, J. Electrochem. Soc. 154 (2007) A971–A977.
[8] Y.-K. Sun, Z. Chen, H.-J. Noh, D.-J. Lee, H.-G. Jung, Y. Ren, S. Wang, C.S. Yoon, S.-T. Myung, K. Amine, Nat. Mater. 11 (2012) 942–947.
[9] H.-J. Noh, Z. Chen, C.S. Yoon, J. Lu, K. Amine, Y.-K. Sun, Chem. Mater. 25 (2013) 2109–2115.
[10] H.-J. Noh, J.W. Ju, Y.-K. Sun, ChemSusChem 7 (2014) 245–252.
[11] J.-W. Ju, E.-J. Lee, C.S. Yoon, S.-T. Myung, Y.-K. Sun, J. Phys. Chem. C 118 (2014) 175–182.
[12] H.-J. Noh, S.J. Youn, C.S. Yoon, Y.-K. Sun, J. Power Sources 233 (2013) 121–130.
[13] Y.-K. Sun, D.-J. Lee, Y.J. Lee, Z. Chen, S.-T. Myung, ACS Appl. Mater. Interfaces 5 (2013) 11434–11440.
[14] M.-H. Lee, Y.-J. Kang, S.-T. Myung, Y.-K. Sun, Electrochim. Acta 50 (2004) 939–948.
[15] Y.-K. Sun, D.-H. Kim, C.S. Yoon, S.-T. Myung, J. Prakash, K. Amine, Adv. Funct. Mater. 20 (2010) 485–491.
[16] Y.-K. Sun, S.-T. Myung, B.-C. Park, J. Prakash, I. Belharouak, K. Amine, Nat. Mater. 8 (2009) 320–324.
[17] D.J. Miller, C. Proff, J.G. Wen, D.P. Abraham, J. Bareno, Adv. Energ. Mater. 3 (2013) 1098–1103.
[18] D.W. Dees, S. Kawauchi, D.P. Abraham, J. Prakash, J. Power Sources 189 (2009) 263–268.